A Fluorine Rich Borate Ionic Additive Enabling High-Voltage Li Metal Batteries

Abstract

Lithium-metal batteries (LMBs) are promising alternatives to state-of-the-art Lithium-ion batteries (LIBs) to achieve higher energy densities. However, the poor cyclability of LMBs resulting from Li metal anode (Li⁰) irreversibility and concomitant electrolyte decompositions limits their practical applications. In this study, we reported a per-fluorinated salt, lithium tetrakis(perfluoro-tertbutyloxy)borate (abbreviated as **Li-TFOB**) as an electrolyte additive for Li metal batteries, which contains 36 F atoms per molecule. This newly designed ionic additive tuned the chemical composition of the solid-electrolyte interphase (SEI) on Li⁰ by increasing the amount of LiF and Li-B-O inorganic species. DFT calculations and Molecular dynamics (MD) simulations indicated the preferential reduction of the **TFOB** anions at Li⁰, which occurs with a lower free energy change than PF₆⁻ anions. The designed ionic additive enables the 4.6 V Li||LiNi_{0.6}Mn_{0.2}Co_{0.2}O₂ (NMC622) cell to achieve an average CE of 99.1% and a high-capacity retention of > 50% after 500 cycles. This experiment-simulation joint study illustrated an attractive approach to accelerating the design of electrolytes and interphases for LMBs.

TOC



Introduction

Lithium-ion batteries (LIBs) have become the dominant power supplies for portable electronics, electric vehicles, and grid-scale energy storage systems. [1, 2] However, because of the constraints imposed by the nature of the intercalation chemistry, present LIBs gradually approach the gravimetric energy density ceiling and fail to meet the expectations of many advanced applications. [1-3] Li metal (Li⁰) is considered the ultimate anode for high energy density batteries owing to its highest theoretical capacity (3860 mAh g⁻¹) and lowest redox potential (-3.04 V vs. standard hydrogen electrode) among all the known candidates. [4] Li metal batteries (LMBs) have been projected as an alternative to LIBs with the potential to achieve high energy densities above 500 Wh/kg. [4]

State-of-the-art electrolytes for LIBs generally consist of lithium hexafluorophosphate (LiPF₆) dissolved in mixed carbonate solvents, such as dimethyl carbonate (DMC), ethylene carbonate (EC), and ethyl methyl carbonate (EMC).^[3] Resulting from the highly reactive nature of Li⁰, the development of LMBs with carbonate electrolytes is troubled with formidable issues, including: (1) continuous and uncontrollable decomposition of carbonate solvents, which are ester by nature and hence intrinsically more susceptible against reduction; (2) growth of dangerous morphologies such as dendritic or dead Li⁰; (3) infinite volume change during the repetitions of Li deposition and stripping processes; and (4) poor Coulombic efficiency (CE), which consumes both Li⁰ inventory and electrolyte irreversibility.^[5-7] Most of these issues are induced by the unstable and non-uniform interphases, known as solid-electrolyte interphase (SEI), formed between Li⁰ and a bulk electrolyte and serving thereafter as a kinetic barrier against the reactions between Li⁰ and the

electrolyte. In recent years, intensive efforts have been devoted to electrolyte engineering to design an ideal SEI to effectively suppress undesirable Li⁰ morphologies and minimize battery irreversibility. Understanding derived from diversified characterizations has shown that an inorganic-rich SEI containing abundant LiF or Li-B-O works better in regulating Li⁰ deposition behaviors, preventing dendritic and dead Li⁰ growth, and improving the cyclability of LMBs.^[8-11]

So far, rational electrolyte designs and engineering that lead to reasonable stability against Li⁰ include highly concentrated electrolytes (HCEs), localized high-concentration electrolytes (LHCEs), fluorinated solvent-based electrolytes, and fluorinated electrolyte additives. [12] These approaches are considered feasible strategies to promote the formation of in-situ fluoride-rich SEI on Li⁰. Among HCEs, such as reported 10.0 M Li bis(fluorosulfonyl)imide (LiFSI) in DMC and 7.0 m LiFSI in fluoroethylene carbonate (FEC) enabled highly reversible Li⁰ plating/stripping owing to the formation of desired Li⁺ solvation structure which minimized the reduction of free solvent molecules and generated fluorinated SEI deriving from either FSI anions or fluorinated solvent molecules on Li⁰ surface.^[9, 13] However, HCEs are typically expensive with high viscosity. low conductivity, and poor separator wettability, which is not suitable for large-scale applications. Fluorinated solvent-based electrolytes and LHCEs, for example, 1.0 M LiPF₆ in a mixture of fluoroethylene carbonate/3,3,3-fluoroethyl methyl carbonate/1,1,2,2-tetrafluoroethyl-2',2',2'trifluoroethyl ether (FEC:FEMC: HFE, 2:6:2 by weight), "full fluorosulfonyl" (FFS) electrolyte, LiFSI in DME and 1,1,2,2-tetrafluoroethyl-2,2,3,3-tetrafluoropropyl ether (TTE) with 1:1.2:3 molar ratio, and 1.0 M LiFSI in fluorinated 1,4-dimethoxylbutane (FDMB) showed high cycling stability in LMBs attributing to the existence of a high degree of fluorination solvent molecules which pre-store a fluorine source and release them upon electrochemical reduction, leading to the in-situ formation of LiF-rich SEI. [4, 14-17] However, most fluorinated solvents reported so far are

not commercially available and require complicated synthesis route. Additionally, these fluorinated solvents generally have a high density (>1.4 g cm⁻³) and thus add an additional dead weight at the expense of the eventual energy density of LMBs.

Unlike HCEs, LHCEs, and other fluorinated solvent-based electrolytes, the application of fluorinated additives is considered more economical and efficient as the amount of it generally is less than 5.0% either by weight or by volume, while its chemical signature in SEIs could be unsymmetrically significant, hence casting prominent influence on the cyclability and cycle life of LMBs, without apparent expenses in cost or other physical properties such as ion transport, viscosity and wettability. [18, 19] Generally, fluorinated additives could be in either molecular (solvent) or ionic (salt) forms, but among the additives described in the literature, molecular additives take an overwhelming percentage.

A recent study reported a fluorinated ionic additive, lithium difluoro(oxalate)borate (LiDFOB) for LMBs. [10] The reductive decomposition of LiDFOB contributed to a LiF-rich interphase which enabled high performance LMBs. The work also detected a B-rich interphase, confirming that an anion could overcome the Coulombic repulsion from Li⁰. In this work, we further explore the possibility of fluorinated ionic additive and report an explicit molecular design strategy to synthesize such a fluorine rich additive, lithium tetrakis(perfluoro-tertbutyloxy)borate (abbreviated as **Li-TFOB**), that assisted in the formation of LiF-rich and B-rich SEI on Li⁰ and supported a high-voltage (4.6 V) LMBs in economic carbonate-based electrolyte.

Design, Synthesis, and Characterization of Li-TFOB

A fluorinated ionic additive is expected to sacrificially decompose and lead to forming a protective SEI between a bulk electrolyte and Li⁰. Such SEI can enable uniform and compact Li⁰

deposition, low cell impedance, and improved battery cyclability. Previously, we reported magnesium and calcium fluorinated borate electrolytes for Mg and Ca batteries^[20, 21] and envisioned lithium fluorinated borate could be employed as functional electrolytes and additives for Li⁰ metal batteries. In this work, a lithium salt with high fluorine density, lithium tetrakis(perfluoro-tertbutyloxy)borate (abbreviated as Li-TFOB), was facilely synthesized by applying nonafluoro-tert-butyl alcohol (C₄F₉OH) as a ligand to react with lithium borohydride (LiBH₄) at room temperature in dimethoxyethane (DME) (Figure 1a). It is anticipated that the high content of the pre-stored fluorine (72wt% or 36 F atoms per molecule) in the anion could have a higher chance of being involved in the formation chemistry of SEI. Because of this giant anion, in which the formal charge is well distributed across the entire structure, it should be able to approach the Li⁰ surface at a higher probability. The synthesized **Li-TFOB** was fully characterized by ¹⁹F-, ¹¹B-, ⁷Li-, ¹³C-NMR, and elemental analysis. **Li-TFOB** displayed a single resonance in the ¹⁹F-NMR (-71.82 ppm), ¹¹B-NMR (-9.14 ppm), and ⁷Li-NMR (-2.38 ppm) spectra (Figures 1b, 1c, and Figure S1a), respectively. With ¹H-NMR and ¹⁹F-NMR spectra for nonafluoro-tert-butyl alcohol (C₄F₉OH) ligand as reference (Figures S2a and S2b), we can determine that the synthesized **Li-TFOB** not only displays expected structure but also exists in high purity. It was found that the highly fluorinated **Li-TFOB** salt has limited solubility in both ether and carbonate solvents (~ 0.1 M), including DME, diglyme (G2), and EC/DMC, which is sufficient for additive applications. It is worth noting that Li-TFOB as an ionic additive has never been reported. Moreover, the ease of one-step synthesis and low costs of reagents endow Li-TFOB for potential large-scale applications.

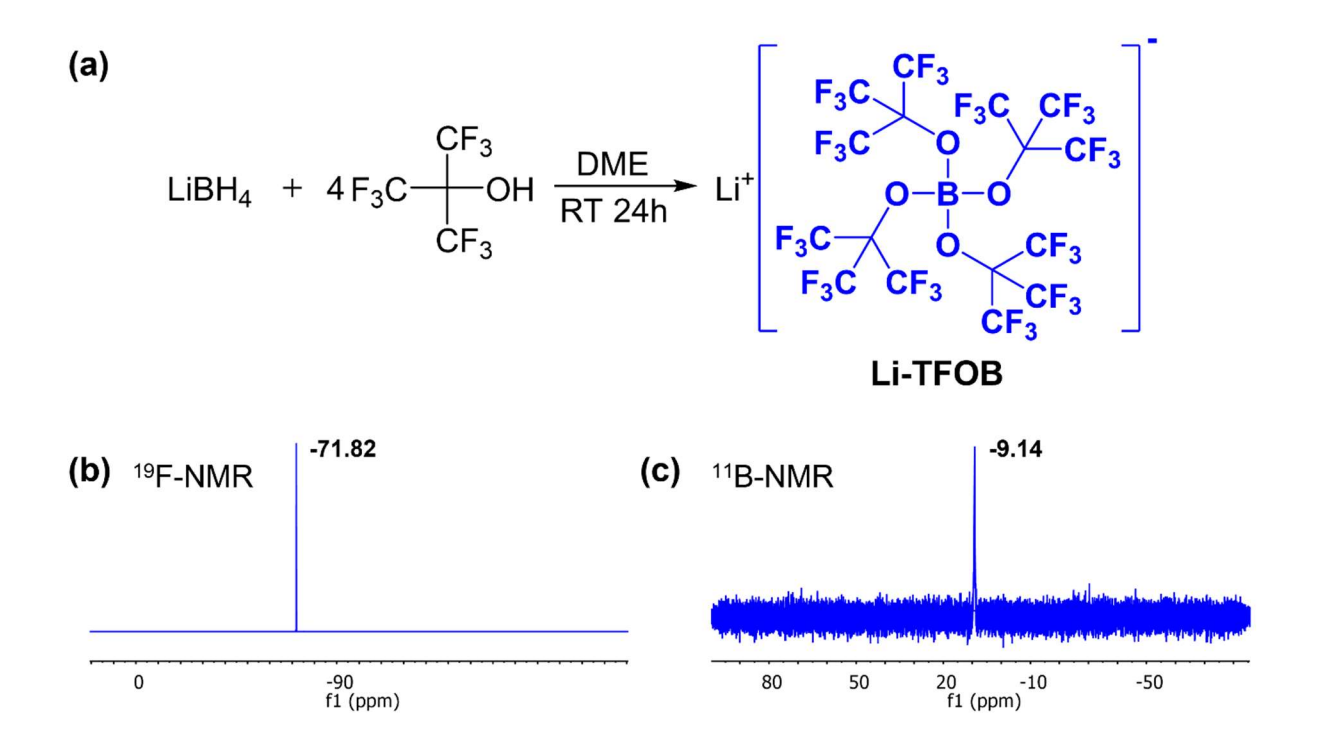


Figure 1. Synthesis and Characterization of **Li-TFOB**. (a) Synthetic route of **Li-TFOB** fluorinated ionic additive; (b)-(c) ¹⁹F-NMR and ¹¹B-NMR spectra of as-prepared ionic additive, respectively. Acetonitrile-d3 was used as the deuterated NMR solvent.

Initial Evaluation of Li-TFOB as An Electrolyte Additive

To evaluate **Li-TFOB** as an additive in battery, LMBs with NMC622 cathodes and Li foil anodes were assembled and tested with four different electrolyte formulations: (1) 1.0 M LiPF₆ in a 1:1 volume ratio of EC and DMC as the baseline, (2) baseline with addition of 2.0 wt% (3.0 mM), (3) 5.0 wt% (8.0 mM), and (4) 10.0 wt% (16.0 mM) **Li-TFOB**, respectively. All tests were conducted in CR2032 coin cells. LiPF₆ in EC/DMC was selected as the baseline, not only because it's the dominant electrolyte used by the current LIBs industry but also because we believe it's the best system to effectively reflect the effectiveness of **Li-TFOB** as an additive, as this carbonate formulation is known for its poor performance with Li⁰ electrode. Ionic conductivities under room

temperature (22 °C) were measured and found to be independent of the electrolyte additive concentration (Figure S3a), with ~12.5 mS cm⁻¹ for all four electrolytes studied, which is reasonable as the amount of additive used should not impact on the bulk ion transport properties, consistent with the previously reported result.^[22] Electrochemical performance was initially quantified in terms of cell specific capacity, Coulombic efficiency (CE), and long-term cycling stability. The addition of the as-synthesized **Li-TFOB** fluorinated salt additive produced remarkable battery performance improvements over the baseline electrolyte, as depicted by the 100 cycling tests in Figure S3b. The improved performances with additive-containing electrolytes were apparently correlated to the different interfacial chemistry on Li⁰ surface.

Closer examination revealed that cells using 5.0 wt% **Li-TFOB** delivered the highest initial discharge capacity (179 mAh g⁻¹) with the best capacity retention (78%) after 100 cycles, as shown in Figures S3c and Figure S3d, respectively. Subsequently, cells with 5.0 wt% **Li-TFOB** additive electrolytes were selected for more detailed investigation.

Electrochemical Evaluation of the Li-TFOB Additive with Li Anode

In order to experimentally evaluate the compatibility between **Li-TFOB** additive and Li⁰, we first assembled symmetric Li||Li cells to confirm the long-term cycling capability of Li⁰ in the baseline and 5.0 wt% **Li-TFOB** electrolytes. As shown in Figure 2a, the symmetric Li||Li cell with the 5.0 wt% **Li-TFOB** electrolyte showed much lower overpotential (ca. 25 mV) for the Li plating/stripping processes compared to the one with the baseline electrolyte (ca. 125 mV). Moreover, the cell with the baseline electrolyte was only stable for about 620 hours (300 cycles) at 0.25 mA cm⁻² with a capacity of 0.25 mAh cm⁻². An abrupt voltage drop-off was observed and is attributed to the rapid formation of hazardous and sharp Li⁰ dendrites causing an internal short circuit (right inset in Figure 2a). In strong contrast, the cycling stability of the symmetric cell with

the 5.0 wt% **Li-TFOB** additive electrolyte was significantly improved without failure even after 1000 hours (500 cycles), indicating that the addition of **Li-TFOB** additive effectively alters the interfacial kinetics that in turn affects Li deposition behavior and the corresponding morphology.

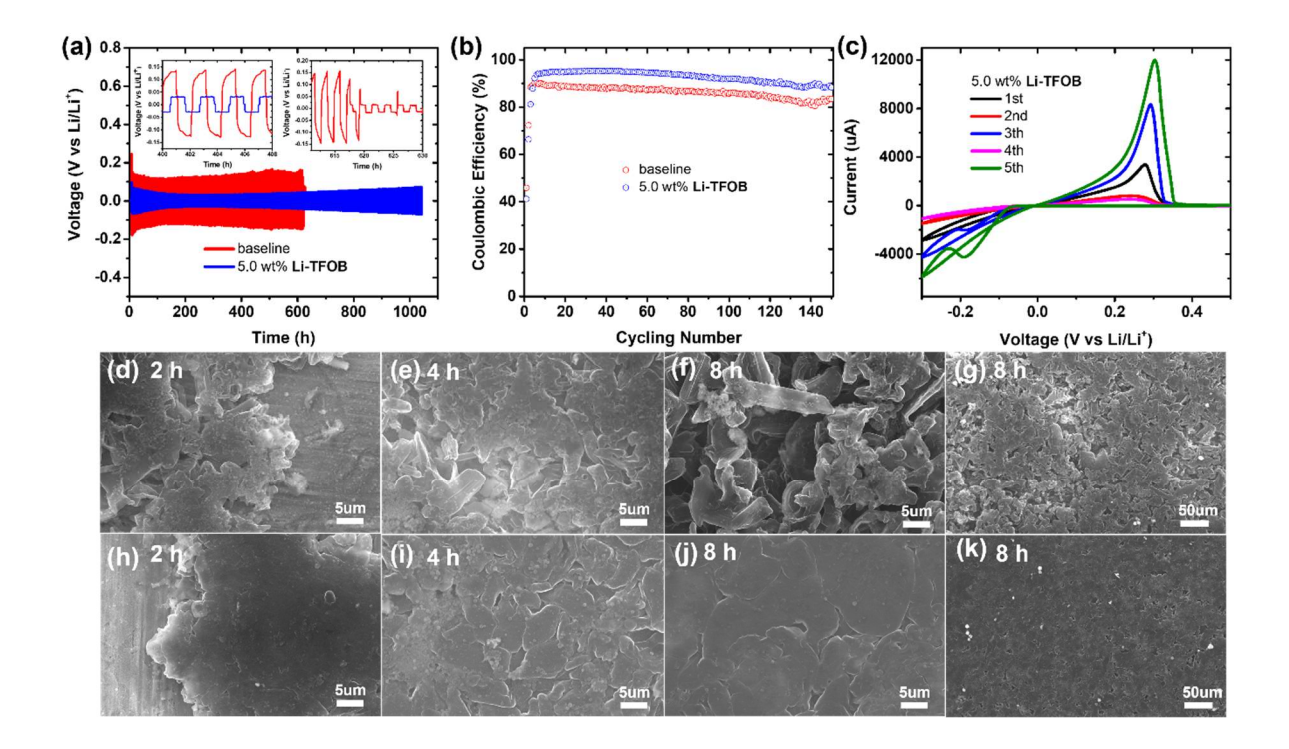


Figure 2. Electrochemical and post-cycling analysis of the **Li-TFOB** additive. (a) Plating/stripping of a Li anode in symmetric Li||Li cells cycled at 0.25 mA cm⁻² with an areal capacity of 0.25 mAh cm⁻²; (b) CE of Li plating/stripping from Li||Cu half-cells at a current density of 0.25 mA cm⁻² with an areal capacity of 0.5 mAh cm⁻²; (c) CV curves for Li plating/stripping between -0.3 V-0.5 V at a scan rate of 2.0 mV s⁻¹ using the 5.0 wt% **Li-TFOB** additive electrolyte; (d)-(g) SEM images for the Li plating morphology on Cu substrates in the baseline electrolyte, (h)-(k) SEM images for the Li plating morphology on Cu substrates in the 5.0 wt% **Li-TFOB** additive electrolyte. For Li plating morphologies study, the applied current density is 0.25 mA cm⁻², 0.5 mAh cm⁻² areal capacity for (d) and (h), 1.0 mAh cm⁻² for (e) and (i), 2.0 mAh cm⁻² for (f), (j), (g), and (k).

To further confirm the effect of the **Li-TFOB** additive, so called "anode-free" cells in Li||Cu configuration were assembled. Figure 2b compares the long-term Li⁰ plating/stripping CE in the baseline and 5.0 wt% **Li-TFOB** additive electrolytes. In the former, the average CE for 150 cycles was below 90.0%, indicating poor reversibility of Li⁰ plating/stripping in carbonate-based electrolytes as a result of the unsuccessful protection provided by the formed SEI. In sharp comparison, with the addition of 5.0 wt% **Li-TFOB**, the CE was increased to 95.0%, revealing a much better Li⁰ plating/stripping reversibility, which was further confirmed using cyclic voltammetry (CV) in the potential range of -0.3 V - 0.5 V in Li||Cu half-cells. As demonstrated in Figure 2c, the current responses in the 5.0 wt% **Li-TFOB** additive electrolyte kept increasing while the baseline electrolyte showed the reverse trend (Figure S5), further verifying the faster reaction kinetics for Li⁰ plating/stripping, which is attributed to the formation of more conductive and fluoride-rich inorganic SEI in the 5.0 wt% **Li-TFOB** additive electrolyte.

Further examination of morphologies of the deposited Li⁰ provides mechanistic insights into why **Li-TFOB** assists in better reversibility (Figure 2d-2k). After applying a current density of 0.25 mA cm⁻² for 2 h (0.5 mAh cm⁻²), highly porous Li⁰ depositions with a significant amount of needle-like crystals with nano-to-micrometer high aspect ratios were generated in the baseline electrolyte (Figure 2d). On the contrary, in the 5.0 wt% **Li-TFOB** additive electrolyte, the deposited Li⁰ adopts a dense and smooth surface, and non-dendritic Li crystal structures were observed (Figure 2h). Due to the limited plating time, a large portion of the Cu substrate was still bare, while Li plating sustained for 4 h (1.0 mAh cm⁻²) and 8 h (2.0 mAh cm⁻²) at current density 0.25 mA cm⁻², SEM images showed full coverage of Cu substrates by deposited Li⁰. After 4 h and 8 h Li plating in the baseline electrolyte (Figure 2e-2f), dendritic as well as dead Li⁰ formed on the surface of Li⁰ electrode, but a more compact and uniform Li⁰ surface was observed in the presence

of 5.0 wt% **Li-TFOB** additive (Figure 2i-2j). SEM images under large magnification (50 um) were also collected. Obviously, as shown in Figurek, the deposited Li⁰ maintained a dense and smooth surface without porous structures in the 5.0 wt% **Li-TFOB** additive electrolyte. However, as depicted in Figure 2a, the highly porous structures and cracking overwhelm the deposited Li⁰ surface in the baseline electrolyte, which is likely due to the consumption of bulk electrolytes with severe and uncontrollable interfacial reactions and loss of active Li. These observations support that **Li-TFOB** is an effective ionic additive that forms protective SEI to regulate a dense and homogeneous Li⁰ deposition, suppress dendrites growth, and mitigate undesirable side reactions, which eventually leads to higher CE and longer cycling life of a Li anode.

X-ray photoelectron spectroscopy (XPS) studies were carried out to analyze how **Li-TFOB** affects interphase chemistry. The signals of F1s, B1s, C1s, and O1s for the Li⁰ anodes recovered from the baseline and 5.0 wt% **Li-TFOB** additive electrolytes were compared (Figure 3a-h). The major difference lies in the significant variations in the abundance of LiF and Li-B-O inorganic species. A higher LiF content was detected in the 5.0 wt% **Li-TFOB** additive electrolyte than in the baseline, as can be seen from F1s spectra (Figure 3a and 3e). On the contrary, in the baseline electrolyte, a larger amount of Li_xPO_yF_z (~687.5 eV, F1s) was observed compared to the 5.0 wt% **Li-TFOB** additive electrolyte, which might be from the decomposed LiPF₆ salts and this trend can be further confirmed in the P2p signal spectra (Figure S6).^[10, 23] On the other hand, the LiF rich SEI generated in the 5.0 wt% **Li-TFOB** additive electrolyte apparently was contributed by the reduction of **Li-TFOB** additive. LiF has been regarded as a critically important SEI component in suppressing Li⁰ dendrites growth and ensuring higher Coulombic efficiency due to its good electronic insulating property and high interfacial energy.^{[14], [23, 24]} Also attributed to the sacrifice of the **Li-TFOB** additive, the signal of a Li-B-O (192.3 eV, Figure 3f) compound was detected in

the 5.0 wt% **Li-TFOB** additive electrolyte, which was also believed to be a beneficial inorganic SEI component inhibiting the consumption of bulk electrolyte and lithium dendrites growth.^[10] Higher amount of Li-B-O compound in the 5.0 wt% **Li-TFOB** additive electrolyte was also confirmed in the O1s signal spectra (Figure 3h). In addition, extensive carbonate decomposition in the baseline electrolyte was also observed in the regions of C1s and O1s (Figures 3c and 3d) as compared to the **Li-TFOB** additive electrolyte (Figures 3g and 3h). Specifically, more organic phases, such as R-(CO₃)-, C-O, and C=O were detected for the baseline electrolyte.

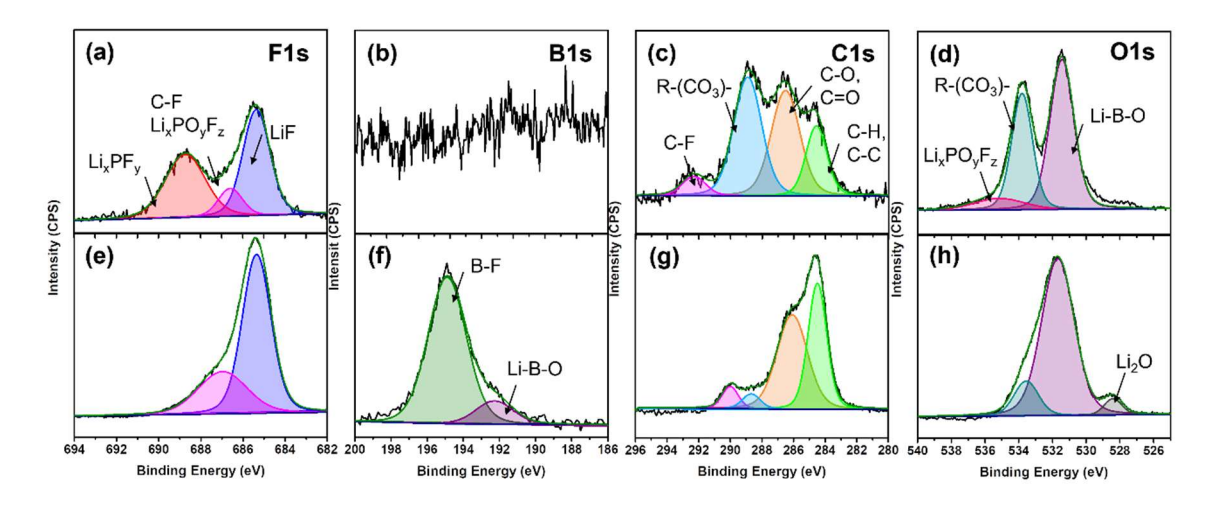


Figure 3. XPS spectra analysis of the SEI components on cycled Li anode surface. (a)-(d) are for a symmetric Li||Li cell after cycling with the baseline electrolyte; (e)-(h) are for a symmetric Li||Li cell after cycling with the 5.0 wt% **Li-TFOB** additive electrolyte.

High-voltage Li Metal Battery using the Li-TFOB Additive

The advantages of the as-designed **Li-TFOB** salt additive were further demonstrated in Li||NMC622 full cells with commercial NMC622 as a cathode and Li⁰ as an anode. The full cell displayed an initial discharging specific capacity of 200.4 mAh g⁻¹ for the 5.0 wt% **Li-TFOB** additive electrolyte, while 180.9 mAh g⁻¹ for the baseline. Compared to the baseline electrolyte,

the full cell with the 5.0 wt% Li-TFOB additive electrolyte brought more stable electrochemical performance, including discharging capacity retention and Coulombic efficiency. As presented in Figure 4a, the 5.0 wt% Li-TFOB additive electrolyte presents better cycling stability, retaining 80% of the original specific discharging capacity after 200 cycles with an average Coulombic efficiency of 99.1%, whereas the full cell with the baseline electrolyte retained <10% capacity retention with fluctuating Coulombic efficiency indicating the poor and unstable interphase falls apart. The fast capacity decay for the pure carbonate-based baseline electrolyte was also reported in Li||NMC811, Li||NCA, Li||NMC442, and Li||NMC333 full cells.[14, 23, 25, 26] The specific discharging capacity retention for the full cell with the 5.0 wt% Li-TFOB additive electrolytes could even be maintained higher than 50% after 500 cycles. Figure S7a and S7b show the representative charge-discharge curves of Li||NMC622 full cells with the baseline and 5.0 wt% Li-**TFOB** additive electrolytes, respectively. Cyclic voltammetry (CV) profiles within the potential range of 2.7-4.6 V for Li||NMC622 full cells are shown in Figure S8, we can see that the current responses in the 5.0 wt% Li-TFOB additive electrolyte are stronger and overlap fairly well after the initial two activation cycles while the current responses in the baseline are weaker and keep decreasing, which is consistent with the results observed in Li||Cu half cells study (Figure 2c). Moreover, the presence of the Li-TFOB additive enabled the full cell to possess a smaller impedance, as revealed by the electrochemical impedance spectroscopy (EIS) of Li|NMC622 cells after cycling (Figure 4b). It is worth noting that Li||NMC622 full-cell using the 5.0 wt% Li-TFOB additive electrolyte also showed the best electrochemical performance compared to those with LiDFOB and LiTFSI additives (Figure S9 and notes).

SEM was also carried out to characterize the detail of Li^0 dendrites growth on anodes cycled in Li||NMC622 full cells (Figure 4c-h). In the baseline electrolyte system, the surface of Li^0 was

cracked (Figure 4c), where a higher magnification SEM image revealed porous structures and dendrites overwhelming the cycled Li⁰ surface morphology (Figure 4d). In sharp contrast, in the 5.0 wt% **Li-TFOB** additive electrolyte, the cycled Li⁰ maintained a dense and smooth surface (Figure 4f). A further zoomed-in SEM image showed non-dendritic Li depositions (Figure 4g), and the morphology is well consistent with the Li deposition study discussed in Figure 2h-2k. Additionally, the thickness of the cycled Li⁰ in the baseline becomes 75.72 um (Figure 4e), while only 45.46 um Li⁰ thickness resulted from the 5.0 wt% **Li-TFOB** additive electrolyte (Figure 4h), due to denser Li⁰ packing enabled by the favorable interphase chemistry, as evidenced by higher Coulombic efficiencies and gravimetric capacity (Figure 4a). The SEM images of surface and cross-section for fresh/uncycled Li⁰ is provided in Figure S10 for comparison.

XPS was also conducted to reveal the cathode electrolyte interphase (CEI) formed on the surface of NMC622 cathode (Figures S10 and S11). The cycled NMC622 with the 5.0 wt% **Li-TFOB** additive electrolyte shows a stronger LiF signal (~685 eV) compared to the baseline electrolyte. Besides, the CEI contents of C-O, C=O, and R-(CO₃)- formed in the 5.0 wt% **Li-TFOB** additive electrolyte is much lower than the baseline indicating a less carbonate solvents decomposition. Moreover, a large amount of Li-B-O and B-F are detected after the addition of **Li-TFOB** (Figure S11), which could be efficient to inhibit the bulk electrolyte decomposition and the dissolution of transition metals in cathode.

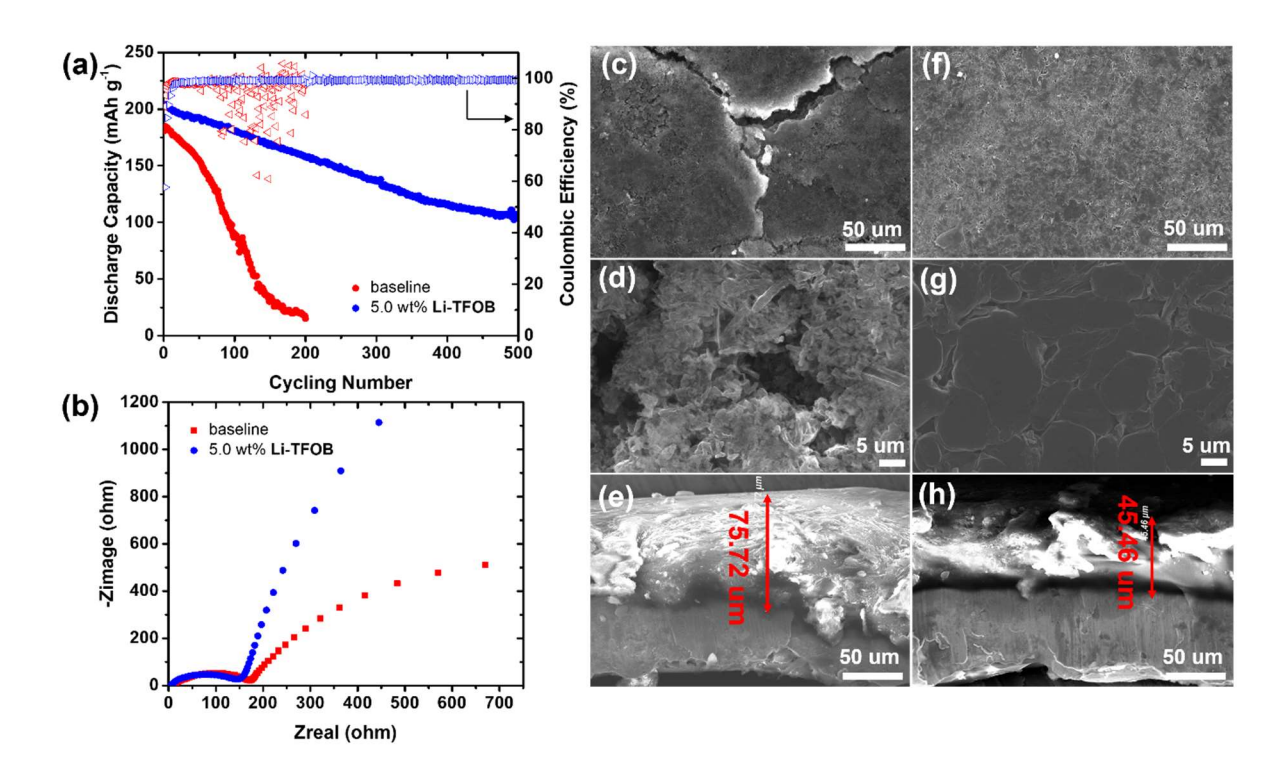


Figure 4. Electrochemical and post-cycling analysis of the Li-TFOB additive in full batteries. (a) Long-term cycling performance of Li||NMC622 full cells in these two electrolytes with 2.7-4.6 V cut off voltage at the current density of 50 mA g⁻¹; (b) EIS spectra of Li||NMC622 full cells after cycling in these two electrolytes; (c)-(d) SEM images of cycled Li anode reclaimed from the baseline; (f)-(g) SEM images of cycled Li anode reclaimed from the 5.0 wt% Li-TFOB additive electrolyte; (e) SEM image of the cross-section of cycled Li anode in the baseline; (h) SEM image of the cross-section of cycled Li anode in the 5.0 wt% Li-TFOB additive electrolyte.

Computational Studies of the Li-TFOB Additive

Density functional theory (DFT) calculations were conducted to shed light on the electrochemical behavior of the **TFOB** anion at Li⁰ surface so that one could infer the reaction pathways leading to the SEI formation. In this study, DFT calculations were performed using B3LYP and M062X functional coupling with the 6-311G++(d,p) basis set.^[27, 28] Considering that experimental characterizations have narrowed down the influence of **Li-TFOB** additive to its

impact on the SEI chemical compositions, the DFT calculations were focused on the reduction reactions of the TFOB anion. [14, 29] Five different types of F atoms can be identified by their distance relative to the central B atom, which is shown via the radial distribution function between B and F (Figure 5a). The relatively larger van der Waals radius of F vs. H atom (1.47 Å vs. 1.20 Å) renders the conformation changes of **TFOB** barely allowable and hence creates an environment where the conformational isomers could be differentiated at a timeframe of pico-second. Such differentiation cannot be observed in NMR spectra (Figure 1) due to the poor temporal resolution (> nano-seconds) of NMR, where all five F types offer one averaged signal. Therefore, the calculations of reduction potentials need to be conducted on each type of F atom. Previous studies have demonstrated the importance of the coordinating environment in determining reduction potentials. [30, 31] Obtaining structural correlations between **TFOB** and all other molecules/ions is straightforward in MD simulations, of which the corresponding radial distribution function (RDF) is shown in Figure 5c. Despite the excess of F atoms, the **TFOB** can be efficiently dissolved by the solvent molecules, i.e., EC and DMC comprising the first solvation shell, in which EC molecules maintained the closer distance to the central B. The first TFOB-Li⁺ RDF peak was located at 10.5 Å with a magnitude of 1.3, indicating no strong correlation between cation and anion. Nevertheless, the **TFOB-**Li⁺ RDF remains non-zero even within the range of the EC/DMC shell, yielding the coordination of 1.9 at 10 Å. Therefore, including extra Li⁺ (not the oxidation product of Li⁰) in the calculation of reduction potential is required. The **TFOB-TFOB** RDF peak magnitude gives a relatively higher value of 1.7 for the first peak. Considering the low concentration of TFOB (5.0 wt%, 8.0 mM), the coordination number (CN) within the first coordination shell is only 0.2, excluding the participation of the second **TFOB** during the reduction. The detailed RDFs and corresponding CNs between Li⁺ and coordinating species are available in

Figure 5d. The first coordination shell of Li⁺ by carbonate oxygen ranges between 1.8 Å and 3.0 Å, while no **TFOB** oxygen atoms are found in the vicinity of cations.

For DFT calculations, we used the SMD (£=20.0) implicit solvation model to represent the solvating environment. In consistence with previous studies, the Born-Haber cycle has been constructed and used for the DFT calculations (Figure 5e). [14, 29, 32] The calculated reduction potentials leading to the formation of Li-F or Li-F-Li are given in Figure 5f, in which E^0_{TFOB/Ll^0} indicates the reduction process including only TFOB and Li⁰, while $E^0_{TFOB/Ll^0/Ll^+}$ represents the reduction including another Li⁺ in the product. The calculations are conducted with B3LYP potential coupling with 6-311G++(d,p) basis set and on the Gaussian16 platform. The E^0_{TFOB/Ll^0} ranges between 2 V and 2.4 V, while the corresponding reduction potential with an additional Li⁺ increases the number by 0 to 0.4 V. All reduction reaction pathways lead to a dramatically higher potential when compared with that of PF₆-, i.e., 1.6 V, rendering the reduction of TFOB much easier than the PF₆-. [14, 33] Therefore, if TFOB exists in the first passivation layer near Li⁰, the reduction reaction of TFOB with Li-F as the product will be prevalent than similar degradation of PF₆- anion.

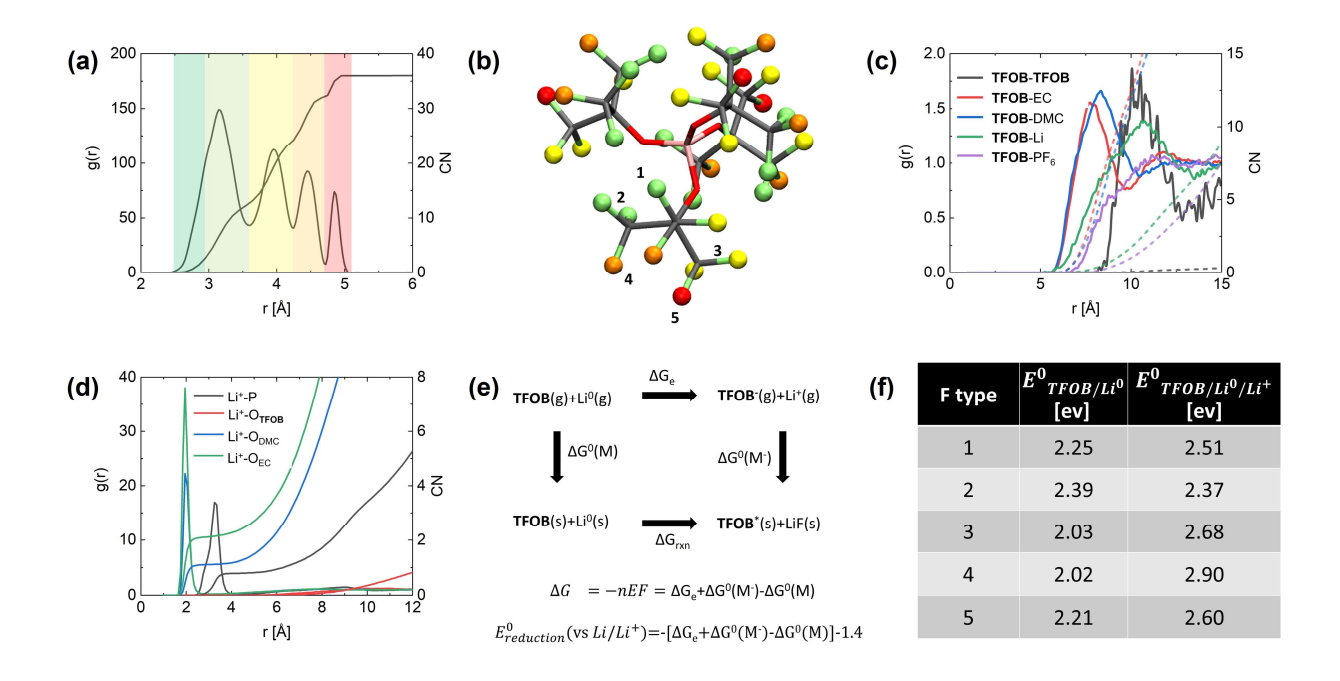


Figure 5. Structural correlations in bulk electrolyte and calculated reduction potentials vs. Li/Li⁺.

(a) intra-molecular structural correlations between B_{TFOB} and F_{TFOB}; (b) illustration of distinguishable F atoms defined by the distance relative to central B atom; (c) inter-molecular structural correlations between **TFOB** and surrounding species and the coordination number of each species is shown in dashed lines indicated by the right y axis; (d) coordinating environment of Li⁺; (e) Born-Haber cycle used to calculate the change in free energies for the electrochemical reactions, when considering the influence of additional Li⁺ the energy terms will be added for reactants, intermediates, and products; and (f) reduction potentials involving distinguishable F atoms illustrated in (b). The **TFOB***(s) refers to the product of **TFOB**- after losing F- and formed LiF.

The simulations of LiPF₆ in EC-DMC 1:1 mixture doped by 5.0 wt% of **Li-TFOB** confined between two parallel electrodes were performed to investigate the electric double layer (EDL) structure. The simulations were conducted at various levels of electric potential differences across the cell. The protocol is consistent with previous studies of EDL structures in supercapacitors and

LIBs. [34, 35] The typical snapshot of the simulation cell can be seen in Figure 6a, in which EC-DMC /LiPF₆ electrolyte doped with the **Li-TFOB** additive is placed between two electrodes. In this study, we calculated the point charge of each electrode atom given by the constant electrode potential simulation that allows charge fluctuation on the electrode atoms, followed by the production runs using the fixed charge method and utilizing the averaged atomic charges obtained from preceding simulations. The EDL potential (U_{EDL}) refers to the potential difference between the electrode surface ($\varphi_{electrode}$) and bulk electrolyte (φ_{bulk}). When electrodes are uncharged, the solvent molecules and electrolyte ions adsorb on the electrode surface and which can result in some potential differences with respect to the bulk electrolyte. The corresponding potential difference is typically defined as the potential of zero charge (PZC). For 1.0 M LiPF₆ dissolved in EC: DMC 1:1 system, the PZC is -0.28 V. [36] Therefore, the electrode potential as the Poisson potential drop across the EDL is calculated using the formula $U=U_{EDL}$ -PZC= $\varphi_{electrode}$ - φ_{bulk} -PZC. To maintain the simulation cell as a charged neutral system, the two electrodes are charged simultaneously with the opposite polarity. The density profiles of solvent molecules in Figure 6b show the passivation of the negatively charged electrode by EC and DMC solvents. Consistent with the previous simulation study, the presence of the less polar DMC molecules decreases with increasing potential, while the density profiles of more polar EC molecules increase with increasing electrode potential.^[37] The presence of solvent in the first interfacial layers, leads to its reduction and formation of organic compounds that are confirmed by the XPS measurement in Figure 3c, 3d, 3g, and 3h.

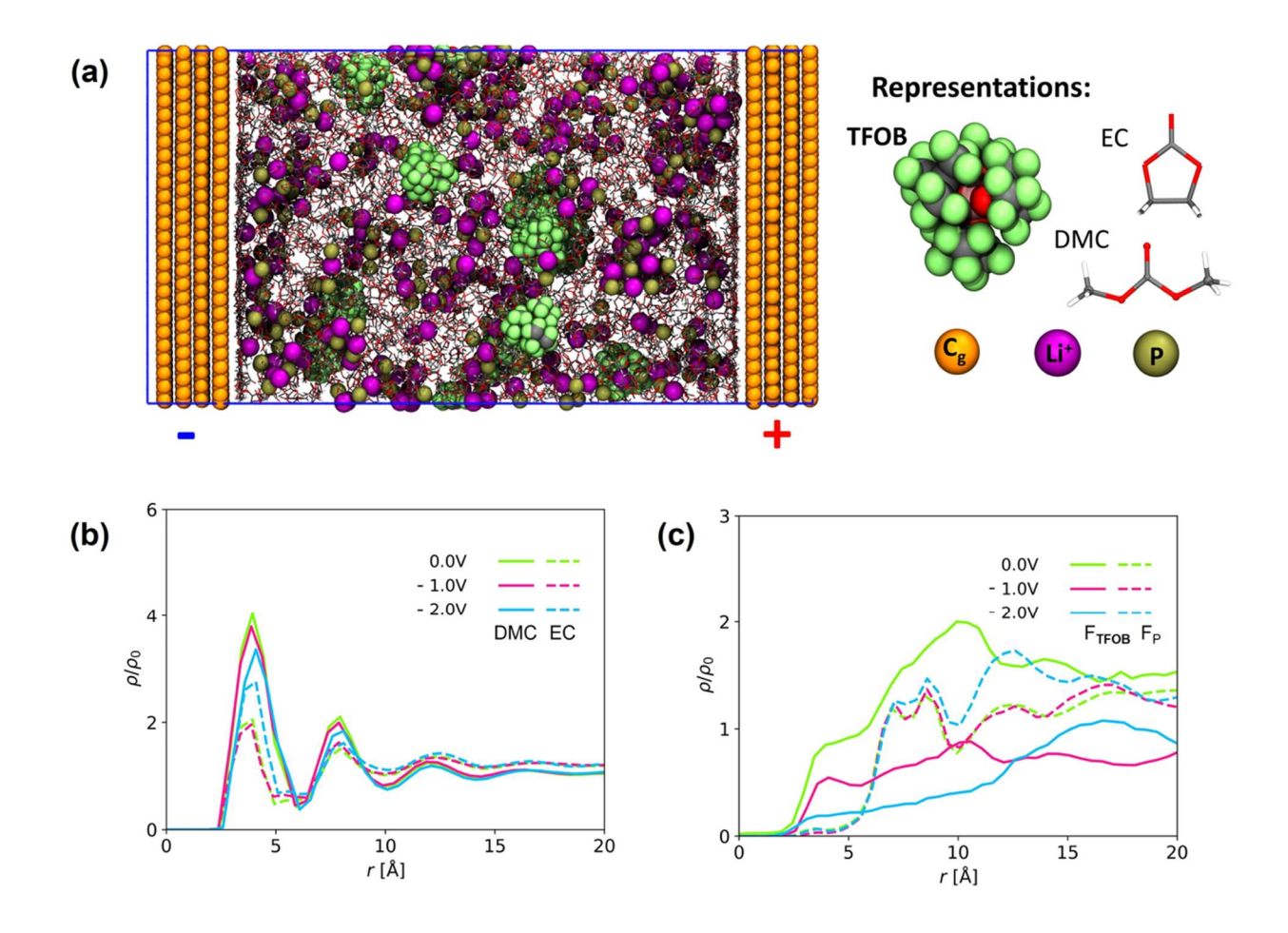


Figure 6. Simulation of electric double layer and structural properties. (a) setup of simulation and a typical snapshot of LiPF₆/EC/DMC with 5.0 wt% **Li-TFOB** additive; (b) density profile Li⁺ and solvent molecules; (c) density profiles of F atoms on **TFOB** and PF₆⁻ near negative electrodes at different levels of electric potentials.

For the formation of LiF-rich SEI, which has been demonstrated as one of the promising strategies to improve the performance of lithium-ion and lithium-metal batteries, [14, 29, 38] the F-containing species (**TFOB** and PF₆⁻) must be present in the EDL to allow sufficient rate of reduction of these compounds. Figure 6c shows the density profiles of F atoms from **TFOB** and PF₆⁻ ions near the negatively charged electrode as a function of electrode potential. The density profiles of F atoms in Figure 6c indicate that F of **TFOB** anion can passivate the negative electrode

and approach it much closer than the F atoms from PF₆-, labeled as F_p. On the negatively charged electrode surface, the first layer of EDL is primarily dominated by Li⁺, while compensating charge anions are located in the further removed layers. Due to the much larger size of the **TFOB** anion, even if its center of mass and charge are located in the outer EDL layer, the peripheral F atoms can still reach the electrode surface. As the magnitude of negative potential on the surface increases, FTFOB atoms exposed to the surface can undergo reduction reactions. Considering the significantly lower reduction potential for **TFOB** than PF₆-, the LiF produced during the reduction of **TFOB** will participate in the formation of SEI at the early stage of battery cycling or even before the battery cycling in the presence of a Li anode.

Conclusions

We designed and synthesized a new ionic additive with per-fluorinated anions, i.e., **Li-TFOB**, whose predominant presence in the interfacial region near Li⁰ grants it a high probability of being reduced and contributing to SEI chemistry. The **Li-TFOB** additive in the LiPF₆ carbonate electrolyte can effectively form a stable LiF-rich SEI to enable the stale cycling of Li⁰ with non-dendritic morphology. Based on the beneficial role of the **Li-TFOB** additive, 4.6 V high-voltage Li-NMC622 cells exhibited remarkably improved cycling stability. The presented novel ionic additive not only presents a new electrolyte material for the development of high energy density Li metal batteries but also provides new guidance to design new electrolytes and interphases.

Supporting Information contains additional experimental details and figures and tables. Supporting Information is available online or from the author.

Acknowledgements We thank the Utah Science Technology and Research initiative (USTAR) for supporting this work. L. Zhang, Q. Wei, and D. Dong thank National Science Foundation (grant

no. 1847674 and 2211824) for supporting their graduate studies. We acknowledge that the NMR studies are supported by NSF's MRI program (grant no. 1429195). D. Dong and D. Bedrov acknowledge the generous allocation of computational resources by Center for High Performance Computing at the University of Utah.

References:

- [1] J. B. Goodenough, K. S. Park, J. Am. Chem. Soc. 2013, 135, 1167-1176.
- [2] M. S. Whittingham, Chem. Rev. 2004, 104, 4271-4302.
- [3] K. Xu, Chem. Rev. 2014, 114, 11503-11618.
- [4] X. Ren, L. Zou, X. Cao, M. H. Engelhard, W. Liu, S. D. Burton, H. Lee, C. Niu, B. E. Matthews, Z. Zhu, C. Wang, B. W. Arey, J. Xiao, J. Liu, J.-G. Zhang, W. Xu, *Joule* **2019**, *3*, 1662-1676.
- [5] J. Janek, W. G. Zeier, *Nat. Energy* **2016**, *1*.
- [6] Y. Liu, Q. Liu, L. Xin, Y. Liu, F. Yang, E. A. Stach, J. Xie, *Nat. Energy* **2017**, *2*.
- [7] X. Zhang, Y. Yang, Z. Zhou, Chem. Soc. Rev. 2020, 49, 3040-3071.
- [8] X.-Q. Zhang, X.-B. Cheng, X. Chen, C. Yan, Q. Zhang, Adv. Funct. Mater. 2017, 27.
- [9] L. Suo, W. Xue, M. Gobet, S. G. Greenbaum, C. Wang, Y. Chen, W. Yang, Y. Li, J. Li, *Proc. Natl. Acad. Sci. USA* **2018**, *115*, 1156-1161.
- [10] T. Deng, X. Fan, L. Cao, J. Chen, S. Hou, X. Ji, L. Chen, S. Li, X. Zhou, E. Hu, D. Su, X.-Q. Yang, C. Wang, *Joule* **2019**, *3*, 2550-2564.
- [11] J. Chen, X. Fan, Q. Li, H. Yang, M. R. Khoshi, Y. Xu, S. Hwang, L. Chen, X. Ji, C. Yang, H. He, C. Wang, E. Garfunkel, D. Su, O. Borodin, C. Wang, *Nat. Energy* **2020**, *5*, 386-397.
- [12] M. Li, C. Wang, Z. Chen, K. Xu, J. Lu, Chem. Rev. 2020, 120, 6783-6819.
- [13] X. Fan, L. Chen, X. Ji, T. Deng, S. Hou, J. Chen, J. Zheng, F. Wang, J. Jiang, K. Xu, C. Wang, *Chem* **2018**, *4*, 174-185.
- [14] X. Fan, L. Chen, O. Borodin, X. Ji, J. Chen, S. Hou, T. Deng, J. Zheng, C. Yang, S. C. Liou, K. Amine, K. Xu, C. Wang, *Nat. Nanotechnol.* **2018**, *13*, 715-722.
- [15] W. Xue, Z. Shi, M. Huang, S. Feng, C. Wang, F. Wang, J. Lopez, B. Qiao, G. Xu, W. Zhang, Y. Dong, R. Gao, Y. Shao-Horn, J. A. Johnson, J. Li, *Energy Environ. Sci.* **2020**, 13, 212-220.
- [16] Z. Yu, H. Wang, X. Kong, W. Huang, Y. Tsao, D. G. Mackanic, K. Wang, X. Wang, W. Huang, S. Choudhury, Y. Zheng, C. V. Amanchukwu, S. T. Hung, Y. Ma, E. G. Lomeli, J. Qin, Y. Cui, Z. Bao, *Nat. Energy* **2020**, *5*, 526-533.
- [17] J. Liu, Z. Bao, Y. Cui, E. J. Dufek, J. B. Goodenough, P. Khalifah, Q. Li, B. Y. Liaw, P. Liu, A. Manthiram, Y. S. Meng, V. R. Subramanian, M. F. Toney, V. V. Viswanathan, M. S. Whittingham, J. Xiao, W. Xu, J. Yang, X.-Q. Yang, J.-G. Zhang, *Nat. Energy* **2019**, *4*, 180-186.
- [18] S. S. Zhang, J. Power Sources **2006**, 162, 1379-1394.
- [19] K. Kim, H. Ma, S. Park, N.-S. Choi, ACS Energy Lett. 2020, 5, 1537-1553.
- [20] J. Luo, Y. Bi, L. Zhang, X. Zhang, T. L. Liu, Angew. Chem. Int. Ed. 2019, 58, 6967-6971.

- [21] K. V. Nielson, J. Luo, T. L. Liu, Batteries & Supercaps 2020, 3, 768-772.
- [22] S. A. Krachkovskiy, J. D. Bazak, S. Fraser, I. C. Halalay, G. R. Goward, *J. Electrochem. Soc.* **2017**, *164*, A912-A916.
- [23] N. Piao, S. Liu, B. Zhang, X. Ji, X. Fan, L. Wang, P.-F. Wang, T. Jin, S.-C. Liou, H. Yang, J. Jiang, K. Xu, M. A. Schroeder, X. He, C. Wang, *ACS Energy Lett.* **2021**, *6*, 1839-1848.
- [24] L. Yu, S. Chen, H. Lee, L. Zhang, M. H. Engelhard, Q. Li, S. Jiao, J. Liu, W. Xu, J.-G. Zhang, *ACS Energy Letters* **2018**, *3*, 2059-2067.
- [25] J. Zheng, M. H. Engelhard, D. Mei, S. Jiao, B. J. Polzin, J.-G. Zhang, W. Xu, *Nature Energy* **2017**, *2*.
- [26] X. Li, J. Zheng, X. Ren, M. H. Engelhard, W. Zhao, Q. Li, J. G. Zhang, W. Xu, *Advanced Energy Materials* **2018**, 8.
- [27] Y. Zhao, D. G. Truhlar, Theor. Chem. Acc. 2007, 120, 215-241.
- [28] R. Krishnan, J. S. Binkley, R. Seeger, J. A. Pople, J. Chem. Phys. 1980, 72, 650-654.
- [29] S. A. Delp, O. Borodin, M. Olguin, C. G. Eisner, J. L. Allen, T. R. Jow, *Electrochim. Acta* **2016**, *209*, 498-510.
- [30] A. Wang, S. Kadam, H. Li, S. Shi, Y. Qi, Npj Comput. Mater. 2018, 4.
- [31] P. Peljo, H. H. Girault, Energy Environ. Sci. 2018, 11, 2306-2309.
- [32] F. Wang, O. Borodin, M. S. Ding, M. Gobet, J. Vatamanu, X. Fan, T. Gao, N. Eidson, Y. Liang, W. Sun, S. Greenbaum, K. Xu, C. Wang, *Joule* **2018**, *2*, 927-937.
- [33] O. Borodin, X. Ren, J. Vatamanu, A. von Wald Cresce, J. Knap, K. Xu, *Acc. Chem. Res.* **2017**, *50*, 2886-2894.
- [34] N. Georgi, A. A. Kornyshev, M. V. Fedorov, J. Electroanal. Chem. 2010, 649, 261-267.
- [35] J. Vatamanu, O. Borodin, M. Olguin, G. Yushin, D. Bedrov, *J. Mater. Chem. A* **2017**, *5*, 21049-21076.
- [36] J. Vatamanu, O. Borodin, G. D. Smith, J. Phys. Chem. C 2011, 116, 1114-1121.
- [37] L. Xing, J. Vatamanu, O. Borodin, G. D. Smith, D. Bedrov, *J. Phys. Chem. C* **2012**, *116*, 23871-23881.
- [38] K. Leung, Phys. Chem. Chem. Phys. **2015**, 17, 1637-1643.